Dynamics of Edge Oscillations and Core Relaxations in Harness

R. Ball 1), W. Horton 2)

1) The Australian National University, Canberra 0200 Australia
2) Institute for Fusion Studies, The University of Texas at Austin, Austin, TX 78712 USA

e-mail contact of main author: Rowena.Ball@anu.edu.au

Abstract. Resistive kink oscillations in magnetic fusion plasmas are usually treated as core localized events, yet there there are several mechanisms by which they may interact with the edge dynamics. In this work an exploratory study is made of a low-dimensional model for the edge dynamics, in which entrainment by sawtooth relaxation oscillations in the core is simulated by a periodic forcing term. The bifurcation structure of the constantly forced model is reviewed, to identify oscillatory behavior that could be beneficially modified by mode-locking to the sawtooth period and amplitude. Some interesting and potentially useful effects of entrainment on the dynamics are shown.

1. Introduction

Magnetic fusion plasmas are strongly driven dissipative flows in which the kinetic energy of small-scale turbulence can drive the formation of large-scale coherent structures such as sheared mass flows. This tendency to self-organise is endemic to flows where Lagrangian fluid elements see globally prevalent or soliton-like two-dimensional velocity fields, and is thought to be due to two linked and consequential attributes of the ideal two-dimensional flow that persist in weakly viscous flows: a second quadratic conserved quantity, mean square vorticity or enstrophy, which allows significant spectral fluxes of energy to large scales (inverse energy cascade) [1, 2].

Quasi two-dimensional fluid motion is also behind natural phenomena involving differential transport such as zonal structuring of planetary flows and the segregation of pebbles washed by the sea on a beach (Fig. 1).

The ability of such flows to organise advected or diffusively transported particles or heat is a fair prospect for achieving directed management of turbulent transport in technologies, but it is only in magnetic fusion plasmas that this potential has been exploited.

In toroidal fusion devices two-dimensional fluid motion structures the flow poloidally and gives rise to confinement or L–H transitions, characterized by dramatic enhancement of sheared zonal flows and suppression of high wavenumber turbulence at the edge that degrades confinement [3], and associated ege-localized modes (ELMs). Two major strands have emerged in the literature on the physics of confinement transitions: (1) They are an internal phenomenon that occurs spontaneously when upscale energy transfer from turbulence to shear flows exceeds nonlinear dissipation [4, 5]; (2) They are due to edge ion orbit losses or induced biasing, the resulting electric field providing a torque which drives shear flows nonlinearly [6, 7, 8].

In this contribution we describe a low-dimensional dynamical model in which these two different strands are effectively unified. We review and explain the bifurcation structure of the model, then examine the the oscillatory dynamics using a periodic power input to the edge po-

FIG. 1 Top left photomontage: On Pebbly Beach, NSW, the sea has sorted and segregated the stones according to size. Top right: A rare cloud over Canberra. Secondary instabilities grow from the edge of this streaming cloud formation, a fast-moving zonal flow. Lower left: Sullivans Creek, Canberra. Kinetic energy cascades from both turbulent and laminar flow regions into coherent structures. (Photos R. Ball.) Lower right: Giant coherent structures in the atmosphere of Jupiter. (Photo NASA.)

tential energy reservoir as a simple prototype for entrainment of edge-localized modes (ELMs) by sawtooth relaxation oscillations in the core.

2. Spatially averaged dynamical model

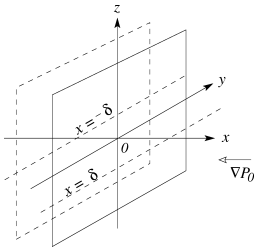

The low-dimensional model is distilled from reduced MHD equations for momentum and pressure convection [9]. In the electrostatic limit these are

$$\rho\frac{d\mathbf{v}}{dt} = -\nabla p + \mathbf{J}\times\mathbf{B} + \mu\nabla_\perp^2\mathbf{v} + \Omega'\tilde{p}\hat{x} - \rho\nu\left(\mathbf{v} - V\left(x\right)\hat{y}\right) \qquad (1)$$

$$\frac{dp}{dt} = \chi\nabla_\perp^2 p, \qquad (2)$$

where $d/dt = \partial/\partial t + \mathbf{v}\cdot\nabla$, together with an incompressibility condition $\nabla\cdot\mathbf{v} = 0$ and a resistive Ohm's law $\mathbf{E} + \mathbf{v}\times\mathbf{B} = \eta\mathbf{J}$. The additional term $\rho\nu\left(\mathbf{v} - V\left(x\right)\hat{y}\right)$ has been included in Eq. 1 to break shear flow reversal symmetry.

Details of the averaging procedure used to obtain a system of three coupled ordinary differential equations from Eqs. 1 and 2 have been given in refs. [10, 11, 13]. Briefly, we use slab geometry as indicated, where the plasma edge region is $-\delta < x < \delta$,with $x = \delta$ at the plasma surface, $\nabla P_0 < 0$ is the y, z-averaged pressure gradient. We extract the dynamics of the mean flow $v_0 = \langle v_y\rangle$, where $\langle\cdot\rangle$ denotes the average over the (y, z) plane, $\mathbf{v} == \mathbf{v}_0 + \tilde{\mathbf{v}}$, by taking the average of Eq. 1 over the (y, z) plane, then multiply by v_0 and integrate over x to obtain the evolution of the background shear flow kinetic energy. The energy moment of Eq. 1 gives the dynamics of the total kinetic energy — shear flow plus fluctuation energy. Potential energy dynamics is obtained by processing Eq. 2 in similar manner.

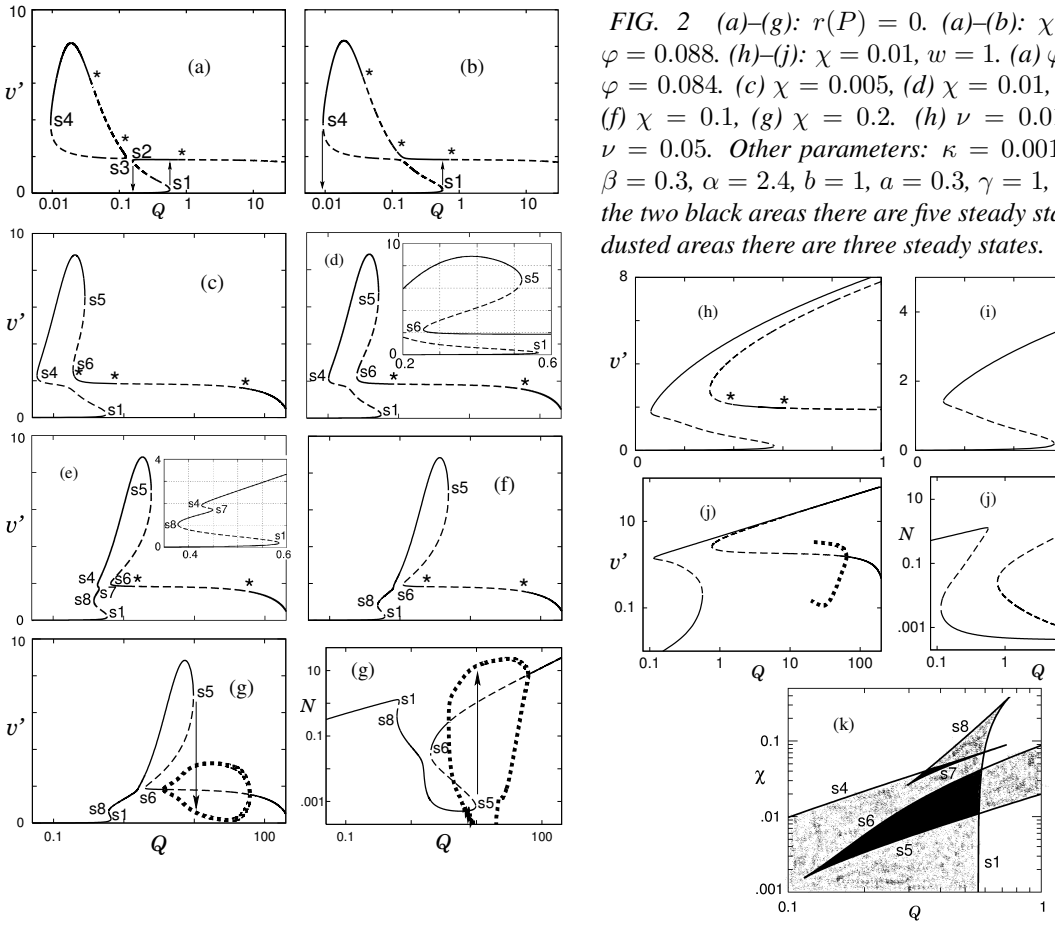

FIG. 2 (a)–(g): $r(P) = 0$. (a)–(b): $\chi = 0$. (c)–(j): $\varphi = 0.088$. (h)–(j): $\chi = 0.01$, $w = 1$. (a) $\varphi = 0.083$; (b) $\varphi = 0.084$. (c) $\chi = 0.005$, (d) $\chi = 0.01$, (e) $\chi = 0.05$, (f) $\chi = 0.1$, (g) $\chi = 0.2$. (h) $\nu = 0.015$, (i) and (j) $\nu = 0.05$. Other parameters: $\kappa = 0.001$, $\varphi = 0.088$, $\beta = 0.3$, $\alpha = 2.4$, $b = 1$, $a = 0.3$, $\gamma = 1$, $\varepsilon = 1$. (k): In the two black areas there are five steady states and in the dusted areas there are three steady states.

This procedure yields a low-dimensional dynamical system in unclosed skeleton form. To close and flesh it out we use approximate expressions for the averaged rates of energy input, transfer, and loss. In general, such averaged rate laws for mass or energy conversions cannot be derived from theory but must be postulated using physical arguments and tested by experiments.

The basic model is further developed and strengthened by interrogating degenerate singularities and matching their unfoldings to appropriate physics. The resulting closed dynamical system is

$$\varepsilon \frac{dP}{dt} = Q - \gamma NP - v'^2 r(P) - \chi P \tag{3}$$

$$\frac{dN}{dt} = \gamma NP - \alpha v'^2 N - \beta N^2 + \kappa v'^2 \tag{4}$$

$$2\frac{dv'}{dt} = \alpha v' N - \mu(P,N)v' + v' r(P) - \kappa v' + \varphi. \tag{5}$$

The variables and parameters are defined in the Table 1, at the end. The rate coefficients may be regarded as lumped dimensionless parameters.

3. Bifurcation structure

It is helpful to review briefly the salient features of the bifurcation structure of Eqs 3–5, some of which have been described previously [12, 13]. Some illustrative bifurcation diagrams of the equilibria are shown in Fig. 2. The power input Q is the control parameter and the diagrams

are rendered for the shear flow variable v' in (a)–(j), and for the turbulent kinetic energy in (g) and (j). (The bifurcation diagrams were computed using the continuation code AUTO [14]. Stable and unstable equilibria are marked with solid and dashed lines respectively. Amplitude envelopes of limit cycle enclaves, which begin at Hopf bifurcations on the equilibrium solution curves, are marked by black dots. Where amplitude envelopes are not marked for clarity, stability changes due to Hopf bifurcations are starred.) In (a) and (b) the thermal diffusivity parameter χ is zero.

In (a), at the given values of the other parameters, an islet of steady-state solutions is formed. From the low shear flow solution branch we make a transition at s1 to an *intermediate* shear flow branch and progress through the onset of an oscillatory regime at the starred Hopf bifurcation. The back-transition occurs at s2. The islet can only be reached via a transient.

In (b) we see a radical difference in the global dynamics: as the power Q is withdrawn the shear flow grows enormously, passes through a second oscillatory regime and the maximum, and **the back-transition at s4 occurs at relatively low power input**.

(c)–(g) are computed for nonzero increasing values of the thermal diffusivity parameter χ.

In (c) two new turning points s5 and s6 have appeared. They were born from a *local* cusp singularity but the *global* effect is to stoop and shift the entire pensinsula towards higher Q. As in (a) and (b) the system transits to an intermediate shear flow state at s1, but from this branch the effect of decreasing Q is radically different: at s6 *another discontinuous transition* occurs to a high shear flow state on the peninsula.

In (d) between s5 and s6 there is a range of fivefold multiplicity, which in (e) has disappeared in a surprisingly mundane way: not through a singularity but merely by the shift of the peninsula toward higher Q. But the shift creates a new and qualitatively different range of fivefold multiplicity through the creation of s7 and s8 at another cusp singularity.

In (f) s4 and s7 have been annihilated at yet another cusp. Thus there are four cusps, the origins of which can be seen in the 2-parameter diagram (k), onto which the lines of s1, s4, s5, s6, s7, and s8 over χ are projected. From the high shear flow branch in (e), (f), and (g), increasing Q induces the system to transit at s5 to a limit cycle

In (g) we see super-suppression of the turbulence N corresponding to this enormous uptake of energy by the shear flow, but the hard onset of oscillations at the s5 transition causes the turbulence to rise again dramatically.

(h)–(j) show the effects of strand (2) confinement transition physics. In Eqs. 3 and 5 $r(P)$ is a competing potential energy conversion channel that can dominate the dynamics when the critical escape velocity w is low or the pressure is high — and this is exactly what we see in the bifurcation diagrams, (h)–(j). The high shear flow peninsula is elongated and flattened. The Hopf bifurcations in (h), where $r(P)$ is small, have disappeared in (i) through a DZE, leaving the intermediate branch unstable until the remaining Hopf bifurcation (j) is encountered. In the transition region the bifurcation diagram begins to look more like the simple S-shaped, cubic normal form schematics featured in numerous papers by earlier authors. However, this **unified** model accounts for shear flow suppression of the turbulence (j), whereas theirs could not, because they had no coupling to the potential energy and turbulence dynamics.

Thus the model predicts behaviors observed repeatably in magnetic fusion experiments, such as shear flow suppresion of turbulence, and hysteretic, non-hysteretic, and oscillatory transitions [11]. It also predicts new behaviors.

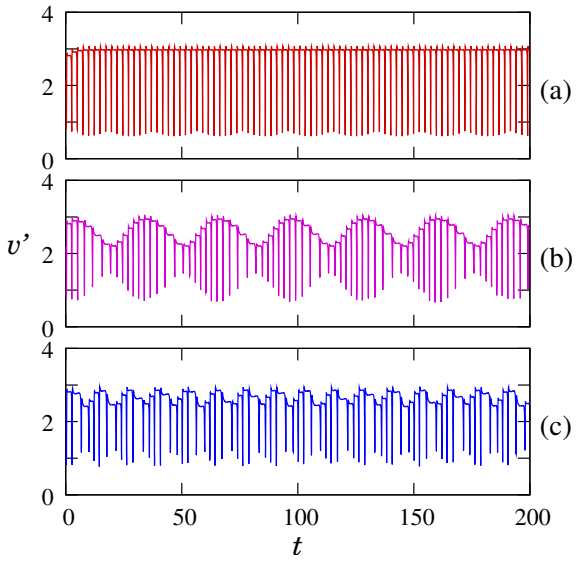

FIG. 3 (a) $Q = 6$, $A_0 = 0$. *(b)* $Q = 4$, $A_0 = 0.5$, $\omega = 0.2$. *(c)* $Q = 4$, $A_0 = 0.5$, $\omega = 0.5$. *Initial data:* $v' = 2.2$, $N = 0.02$, $P = 20$. *Other parameters:* $\kappa = 0.001$, $\varphi = 0.084$, $\varepsilon = 1$, $\gamma = 1$, $\alpha = 2.4$, $\beta = 0.3$, $b = 1$, $a = 0.3$, $\chi = 0$, $r(P) = 0$.

4. Core-edge coupling

In the core of auxiliary heated tokamak plasmas the ineluctable rhythm of slow buildup and rapid conversion of potential energy governs electron and heat radial transport. The growth phase of the sawtooth is accompanied by significant reconnection, then during the collapse the temperature and density in the core fall dramatically [15]. Although the timing and mechanism of the sawtooth collapse are still not completely understood, there is evidence in reversed field pinch devices that ensuing energy fluxes can affect flow shear and confinement at the edge and the oscillatory behavior usually known as edge-localized modes (ELMs) [16, 17]. This suggests that we may regulate edge localized modes by harnessing the natural or engineered sawtooth period and amplitude.

In the simplest prototype for coupled core–edge dynamics we model the sawtooth crash as a periodic power input to the edge potential energy reservoir. This is effected by coupling Eq. 3 to the dynamical system

$$\dot{u} = u(1 - u^2 - x^2) - \omega x \tag{6}$$

$$\dot{x} = x(1 - u^2 - x^2) + \omega u, \tag{7}$$

which has an asymptotically stable periodic solution $(u(t), x(t)) = (\cos(\omega t + \theta), \sin(\omega t + \theta))$, where ω is the sawtooth frequency and θ is an arbitrary phase-shift. Equation 3 becomes

$$\varepsilon \frac{dP}{dt} = Q(1 + A_0 u) - \gamma N P - v'^2 r(P) - \chi P, \tag{8}$$

where A_0 is related to the density amplitude of the core relaxations. Expressing the periodically forced system as Eqs 6–8 is a trick that allows us to monitor the local stability of periodic solutions by computing the eigenvalues of the monodromy matrix, called Floquet multipliers [18]. The variables u and x have no physical significance.

Figure 3 shows the effects of periodic forcing on the self-sustained limit cycle oscillations in the intermediate shear flow regime in Fig. 2(b). These emulate the grassy ELMs that are often seen in high confinement modes. They are regular in (a), albeit with a somewhat scalloped lower envelope. Periodic forcing locks them strongly in (b), a feature that could be useful for selecting times for impurity exhaustion. However, as is expected from three- or higher-dimensional dynamics, the mode-locked dynamics can become very complex (c).

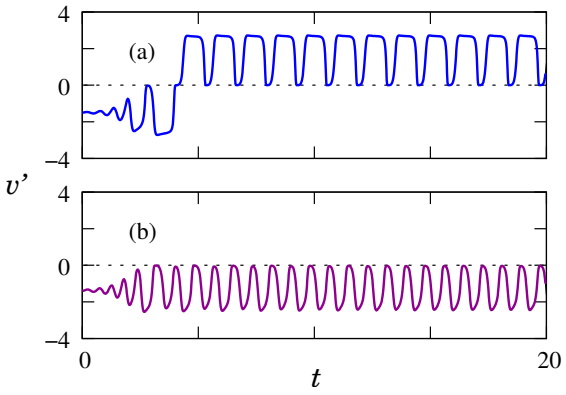

FIG. 4 *(a)* $Q = 70$, $A_0 = 0$. *(b)* $Q = 60$, $A_0 = 22$, $\omega = 1$. *Initial data:* $v' = -1.4$, $N = 11$, $P = 7.97$. *Other parameters:* $\kappa = 0.001$, $\varphi = 0.084$, $\varepsilon = 5$, $\gamma = 1$, $\alpha = 2.4$, $\beta = 0.3$, $b = 1$, $a = 0.3$, $\chi = 0$, $r(P) = 0$.

In Fig. 4 time series are plotted for zero (a) and nonzero (b) A_0 and ω. In this example dissipation is poor, effective capacitance is high, and the symmetry-breaking shear flow drive φ is positive. The initial condition is an unstable solution within the enclave of limit cycles on the $v' < 0$ branch, but there is a spontaneous reversal of shear flow (a) before the dynamics can settle onto a limit cycle on the $v' > 0$ branch. We see that a periodic power input (b) can suppress this reversal.

Figure 5 shows another effect of periodic forcing on an initial transient. Here the system is evolved from an unstable solution near the upper Hopf bifurcation on the peninsula in Fig. 2(b). Since the branches of limit cycles emanating from these Hopf bifurcations terminate at homoclinic bifurcations rather than form an enclave, the trajectory must move onto the only stable attractor, which is a solution on the low shear-flow branch. Thus achieving and maintaining a state on the peninsular, super-suppressed branch could be problematic. Where the periodic forcing amplitude A_0 is zero (a) the system relaxes quickly to the low shear-flow branch. The periodically forced system (b) settles into a long train of oscillations before relaxing, giving a longer window of super-suppressed behavior.

5. Discussion

A self-structuring quasi two-dimensional flow such as a magnetic fusion plasma may be structured further by a periodic power input. We have used a periodic forcing term in a low-dimensional model for edge behavior in fusion plasmas to make a preliminary feasibility study of mode-locking by sawtooth oscillations in the core. Some potentially useful effects of periodic forcing on the dynamics are shown. This simple emulation indicates that more detailed modeling using the electron temperature gradient transport model in [19] would be fruitful. The model will also be refined to include a time delay, and modulation of the edge dynamics through inductive and MHD coupling will be investigated.

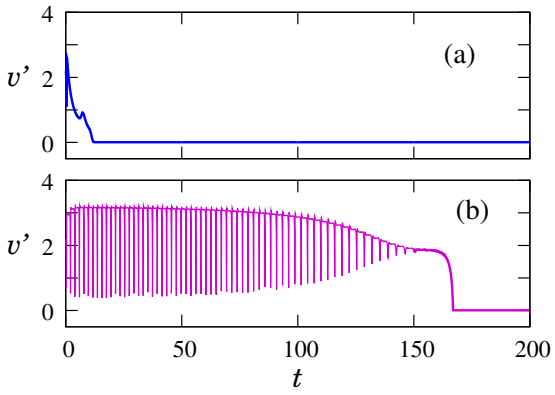

FIG. 5 *(a)* $Q = 0.09$, $A_0 = 0$. *(b)* $Q = 0.09$, $A_0 = 100$, $\omega = 0.01$. *Initial data:* $v' = 2.2$, $N = 0.02$, $P = 20$. *Other parameters:* $\kappa = 0.001$, $\varphi = 0.084$, $\varepsilon = 1$, $\gamma = 1$, $\alpha = 2.4$, $\beta = 0.3$, $b = 1$, $a = 0.3$, $\chi = 0$, $r(P) = 0$.

εP	potential energy in the pressure gradient	ε	thermal capacitance
N	turbulent kinetic energy	F	shear flow kinetic energy
$v' = \pm\sqrt{F}$	poloidal shear flow	Q	power input to the pressure gradient
γ	turbulence growth rate coefficient	χ	cross-field thermal diffusivity
κ	downscale energy transfer rate coefficient	α	Reynolds stress energy transfer rate
β	turbulent energy dissipation rate coefficient	φ	shear flow driving rate
$\mu(P,N)$ $= bP^{-3/2} + aPN$	neoclassical and turbulent viscosities	$r(P)$ $= \nu\exp\left[-\left(w^2/P\right)^2\right]$	ion orbit loss rate
ν	collision frequency	w	critical escape velocity

Table 1.

References

[1] R. H. Kraichnan and D. Montgomery. Two-dimensional turbulence. *Reports on Progress in Physics*, 43:547–619, 1980.

[2] Tabeling P. Two-dimensional turbulence: a physicist approach. *Physics Reports — Review Section of Physics Letters*, 362(1):1–62, 2002.

[3] P. W. Terry. Suppression of turbulence and transport by sheared flow. *Reviews of Modern Physics*, 72(1):109–165, 2000.

[4] P. H. Diamond and Y.-B. Kim. Theory of mean poloidal flow generation by turbulence. *Phys. Fluids B*, 3:1626–1633, 1991.

[5] E-J. Kim, P. H. Diamond, and T. S. Hahm. Transport reduction by shear flows in dynamical models. *Physics of Plasmas*, 11(10):4554–4558, 2004.

[6] S.-I. Itoh and K. Itoh. Model of *L*- to *H*-mode transition in tokamak. *Phys. Rev. Lett.*, 60(22):2276–2279, 1988.

[7] K.C. Shaing and E.C. Jr Crume. Bifurcation theory of poloidal rotation in tokamaks: a model for the L–H transition. *Phys. Rev. Lett.*, 63(21):2369–2372, 1989.

[8] S Magni, C. Riccardi, and H. E. Roman. Statistical investigation of transport barrier effects produced by biasing in a nonfusion magnetoplasma. *Physics of Plasmas*, 11(10):4564–4572, 2004.

[9] H. R. Strauss. Dynamics of high β tokamaks. *The Physics of Fluids*, 20(8):1354–1360, 1977.

[10] H. Sugama and W. Horton. L–H confinement mode dynamics in three-dimensional state space. *Plasma Phys. Control. Fusion*, 37:345–362, 1995.

[11] R. Ball, R. L. Dewar, and H. Sugama. Metamorphosis of plasma shear flow–turbulence dynamics through a transcritical bifurcation. *Phys. Rev. E*, 66:066408–1–066408–9, 2002.

[12] R. Ball. Suppression of turbulence at low power input in a model for plasma confinement transitions. *Physics of Plasmas*, 12:090904–1–8, 2005.

[13] R. Ball. Distilled turbulence. A reduced model for confinement transitions in magnetic fusion plasmas. Proceedings of the Workshop on Turbulence and Coherent Structures in Fluids, Plasmas, and Granular Flows, 10–13 January 2006, Canberra. To be published by World Scientific, Singapore.

[14] The bifurcation diagrams were computed numerically using the continuation code AUTO, see http://indy.cs.concordia.ca/auto/.

[15] J. A. Wesson. Sawtooth oscillations. *Plasma Phys. Control. Fusion*, 28(1A):243–248, 1986.

[16] B. E. Chapman, A.F. Almagri, J. K. Anderson, C. S. Chiang, D. Craig, G. Fiksel, N. E. Lanier, S. C. Prager, J. S. Sarff, M. R. Stoneking, and P. W. Terry. E x B flow shear and enhanced confinement in the Madison Symmetric Torus reversed-field pinch. *Physics of Plasmas*, 5(5):1848–1854, 1998.

[17] A. Kirk, private communication.

[18] R. Seydel. *Practical Bifurcation and Stability analysis. From Equilibrium to Chaos.* Springer-Verlag, New York, 1994.

[19] W. Horton, H.V. Wong, P.J. Morrison, A. Wurm, J.H. Kim, J.C. Perez, J. Pratt, G.T. Hoang, B.P. LeBlanc, and R. Ball. Temperature gradient driven electron transport in NSTX and Tore Supra. *Nuclear Fusion*, 45:976–985, 2005.

Acknowledgment: This work is supported by the Australian Research Council. Part of this work was carried out while RB was a visitor at Politecnico di Torino, partially supported by a Lagrange Fellowship.